

# On the Experiments about the Nonprehensile Reconfiguration of a Rolling Sphere on a Plate

Diana Serra<sup>1</sup>, Joel Ferguson<sup>2</sup>, Fabio Ruggiero<sup>1</sup>, Andrea Siniscalco<sup>3</sup>, Antoine Petit<sup>4</sup>,  
Vincenzo Lippiello<sup>1</sup>, Bruno Siciliano<sup>1</sup>

**Abstract**—A method to reconfigure in a nonprehensile way the pose (position and orientation) of a sphere rolling on a plate is proposed in this letter. The nonholonomic nature of the task is first solved at a planning level, where a geometric technique is employed to derive a Cartesian path to steer the sphere towards the arbitrarily desired pose. Then, an integral passivity-based control is designed to track the planned trajectory. The port-Hamiltonian formalism is employed to model the whole dynamics. Two approaches to move the plate are addressed in this paper, showing that only one of them allows the full controllability of the system. A humanoid-like robot is employed to bolster the proposed method experimentally.

## I. INTRODUCTION

Roughly speaking, manipulation tasks deal with the change of pose of an object between two different configurations. These tasks may be pursued either in a prehensile or in a nonprehensile way, depending on the type of the applied constraints: bilateral in the former case, unilateral in the latter [1], [2]. Within nonprehensile manipulation, the object can still be manipulated by the hand, but it is not possible to prevent any infinitesimal motion of the object, and it is not possible to resist all external wrenches applied to it. For instance, if a person holds an object in the palm, the object cannot fall, but it is not possible to resist any force lifting up the object.

Nonprehensile manipulation is typically considered at a dynamic level since the dynamics of both the object and the robot manipulator are essential to finalize the task. Within dynamic manipulation, a relevant role is played by forces and accelerations, which are used together with kinematic, static and quasi-static forces to achieve a general description of the manipulation task. In general, nonprehensile dynamic manipulation offers some potential advantages over prehensile manipulation such as reduction of the task execution time; extension of the workspace of the robot; increased dexterity of the robotic system; cheap and simple design of

grippers; minimal deformation of the manipulated objects, and so on [2]. On the other hand, the complexity of such nonprehensile tasks leads to dividing them in simpler *manipulation primitives* [2], such as rolling [3], [4], batting [5], [6], juggling [7], [8], [9].

This paper is focused on a specific nonprehensile manipulation primitive: the pose reconfiguration of a sphere rolling on a plate, which is in turn actuated by a robot. As evident from the state of the art in the next section, the examined task has already been extensively investigated. The reason is that the pose reconfiguration of a sphere rolling on a plate is an application including a nonholonomic constraint. Such a task is also fascinating from a control viewpoint: as a matter of fact, there is no smooth feedback asymptotically stabilizing a single equilibrium solution, since Brockett's necessary condition for smooth stabilization is not satisfied [10]. Therefore, the nonholonomic constraint can be handled in two different ways: at the planning level, in which a geometric path is found to reconfigure the whole pose of the sphere; at a control level, in which time-varying or non-smooth feedback control laws are designed. The former approach is contemplated in this paper.

The conceptual flow diagram of the employed algorithm for the rolling sphere reconfiguration is depicted in Fig. 1. The first stage is based on a geometric planner and provides both a Cartesian path and an associated trajectory satisfying the desired position and orientation goal for the sphere. Due to the nature of the nonprehensile manipulation, there is freedom associated with how the ball and plate system is controlled to follow the trajectory of the geometric planner. The controllability of the systems using either force or torque inputs is examined. By supposing that the rolling dynamics is slower with respect to the sample time of the controlled robot, a time-scale separation is considered between the robot and the rolling dynamics. Therefore, only the dynamic model of the ball rolling on the plate is taken into account for control purposes. A simplified model is derived using the port-Hamiltonian (pH) formalism considering fictitious forces applied directly to the rolling sphere as virtual inputs. An Integral Passivity-Based Control (IPBC) is designed to track the trajectory resulting from the previous stage. Control allocation is intended to map the virtual inputs to the real ones actuating the plate. Experiments to verify the results are performed on the humanoid-like robot, shown in Fig. 2.

At the best of the authors' knowledge, this paper proposes some novelties from both the control and the experimental point of views. First of all, the whole dynamic model of both

The research leading to these results has been supported by the RoDyMan project, which has received funding from the European Research Council FP7 Ideas under Advanced Grant agreement number 320992. The authors are solely responsible for the content of this manuscript.

<sup>1</sup>D. Serra, F. Ruggiero, V. Lippiello and B. Siciliano are with CRE-ATE Consortium and with the Department of Electrical Engineering and Information Technology, University of Naples Federico II, via Claudio 21, 80125, Naples, Italy.

<sup>2</sup>J. Ferguson is with School of Electrical Engineering and Computing and PRC CDSC, The University of Newcastle, Callaghan, NSW 2308, Australia.

<sup>3</sup>A. Siniscalco is with ALTEN Italia, via Guelfa 5, Bologna, Italy.

<sup>4</sup>A. Petit is with INRIA, Mimesis Group, 1, place de l'Hopital, Strasbourg, France.



Fig. 1. Conceptual flow diagram of the algorithm.

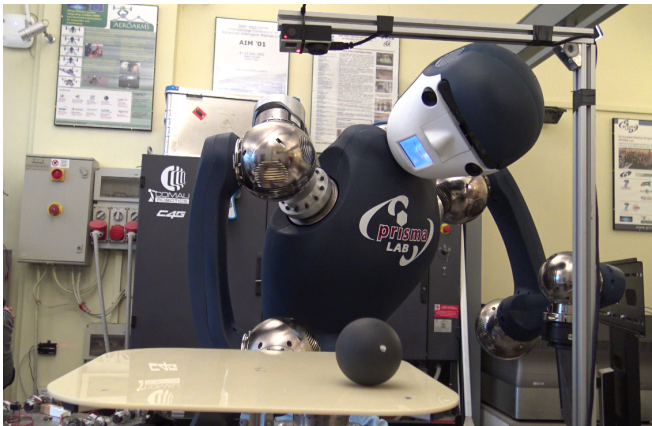


Fig. 2. Picture of the employed 21-dof humanoid-like robot.

the plate and the rolling ball position of the sphere has been taken into account to analyze controllability issues related to the actuated platform. For instance, it has been shown that by actuating the plate with only linear forces it is possible to control the position of the ball on the plate, while the plate has an uncontrolled drift in the space. However, by actuating the plate with only two torques, it is possible to sufficiently control both the plate and the position of the rolling sphere. Moreover, the pH-based scheme proposed in [11] has been modified with the addition of a damping term to improve transient performance: experimental comparison with a standard PID controller has also been carried out. Finally, the authors believe that the performed experiments are the first ones considering a complete nonprehensile reconfiguration of the pose of a rolling sphere on a plate. As from the next section, other nonprehensile experiments in the literature have considered only a re-positioning of the rolling ball.

## II. RELATED WORKS

Montana proposes one of the first mathematical derivations of the kinematics of rolling contact in [12]. Exploiting the chart representation and differential geometry tools, Montana describes the motion of a contact point over the surfaces of two objects in contact. This way of modeling has been exploited, for instance, in the rolling manipulation of a sphere between two fingertips [13]. In the same way, it is worth pointing out that many works in the robotics and control community focus on the rolling sphere reconfiguration task but mainly in a prehensile fashion, obtained by enclosing the sphere between two plates [14], [15], [16], [17], [18]. Usually, one plate is actuated while the other one is fixed. In these prehensile applications, the motion of the contact point can be limited to a subset of the sphere surface, coping with the local nature of the chart representation.

Among the prehensile applications of the ball and plate problem, the simultaneous position and orientation open-loop reconfiguration of a sphere rolling between two horizontal planes has been inspected in [14]. By exploiting the maximum principle, a path is designed to minimize the energy spent by the moving plate. The optimal solution curve minimizes the integral of the geodesic curvature. A more recent work, instead, presents a set-up with only one plate with magnetic actuation [15]. The presence of magnets allow the possibility to counteract external wrenches applied on the ball: this fits the definition of bilateral constraint and, for this reason, the manipulation system can be considered as prehensile<sup>1</sup>. The proposed approach is robust to sphere radius variations. A robotic mechanism equipped with three actuators and tactile feedback is designed in [16] to dexterously manipulate a sphere through prehensile rolling, while in [17] the results have been extended to unknown objects. Furthermore, controllability issues of the prehensile rolling manipulation problem are addressed in [18], where an approximate planning technique employing a mapping to transform the system into a triangular form is proposed.

Examples of robotic nonprehensile rolling manipulation of a sphere rolling on a plate can be found in the literature, but only coping with re-positioning purposes. The position control of a basketball on a plate is tackled in [19]. The linear velocity of the basketball is estimated exploiting a force-torque sensor mounted on the end-effector of a robot manipulator. By using Montana's equations, a method to control a manipulator to follow a planned position trajectory for a spheroidal object is addressed in [20]. A stable contact region is defined on the object's surface, where the neighborhood equilibrium - a concept proposed in [21] - is always guaranteed. Experiments are proposed considering a rubber hemisphere-plate system. An analysis of the kinematics of rolling, based on a coordinate-free approach, reviewing the cases of either pure rolling (non-slipping and non-twisting) or twist-rolling motion, is proposed in [22].

Similarly to this paper, the above-cited articles deal with the nonholonomic constraint at a planning level. Nevertheless, it is worth citing those works solving the prehensile problem at a control level, like the design of time-varying [23], [24], or non-smooth [25], or switching [26] feedback control laws.

## III. GEOMETRIC TRAJECTORY PLANNER

The nonholonomic nature of the ball and plate application is here solved at a planning level. Hence, the trajectory planner proposed in [15] is employed to find the proper path to reconfigure the sphere to the desired pose.

Let  $\Sigma_w : O_w - \hat{x}\hat{y}\hat{z}$  be the world frame, while let  $\Sigma_p : O_p - \hat{x}_p\hat{y}_p\hat{z}_p$  be the frame attached to the plate. The position of the ball in  $\Sigma_p$  is denoted by  $\mathbf{r}_b^p = [x \ y \ \rho]$ , with  $\bar{\mathbf{q}} = [x \ y]^T$  the projection of  $\mathbf{r}_b^p$  on the plate, and

<sup>1</sup>Referring to the example given in the Introduction, it is not possible for a human to resist any force lifting up an object held in the palm. In case of magnets, instead, the magnetic field can withstand forces (within a defined magnitude) trying to lifting up the metal sphere from the plate.

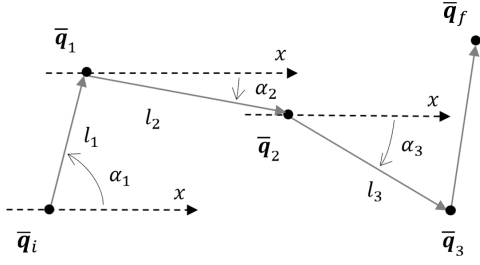


Fig. 3. Scheme of the Cartesian path to link two position and orientation configurations of the rolling sphere.

$\rho \in \mathbb{R}^+$  the radius of the ball. The orientation of the sphere is described by a set of ZYZ Euler angles,  $\phi = (\theta, \phi, \psi)$ . By this convention, any rotation of the sphere,  $\mathbf{R} \in SO(3)$ , can be seen as the combination of three elementary rotations  $\mathbf{R} = \mathbf{R}_{\hat{z}_p}(\theta)\mathbf{R}_{\hat{x}_p}(\phi)\mathbf{R}_{\hat{z}_p}(\psi)$ , where  $\mathbf{R}_{\hat{x}_p}(\cdot), \mathbf{R}_{\hat{z}_p}(\cdot) \in SO(3)$  are elementary rotation matrices around the  $\hat{x}_p, \hat{z}_p$  axes of  $\Sigma_p$ , respectively. The orientation of the ball can alternatively be parameterized by  $\mathbf{R}(\rho\phi - \rho\pi, \theta)\mathbf{R}(\rho\pi, (\theta - \psi)/2)$ , where the rolling motion primitive  $\mathbf{R}(l, \alpha) \in SO(3)$  is defined in [15] as a rotation of  $l$  along the line creating an angle  $\alpha \in \mathbb{R}$  with the  $\hat{x}_p$ -axis. Thus, the sphere can be reoriented into any orientation via two consecutive rolling stages. Likewise, the sphere can be relocated into any position preserving the initial orientation with two more straight rolling stages of a distance of  $2\pi n\rho$ , with  $n \in \mathbb{Z}$ .

To recap, the first two movements re-orient the ball into the desired orientation, while the last two movements lead the ball towards the desired position preserving the reached orientation. In total, the ball performs 4 segments to achieve the desired pose  $\mathbf{q}_f = [x \ y \ \theta \ \phi \ \psi]^T$ . Hence, starting from  $\mathbf{q}_i$ , the sphere has to pass through three intermediate points on the plate ( $\bar{\mathbf{q}}_1, \bar{\mathbf{q}}_2, \bar{\mathbf{q}}_3 \in \mathbb{R}^2$  in  $\Sigma_p$ ), as depicted in Fig. 3. Assuming, without loss of generality, that the initial configuration of the sphere is  $\mathbf{q}_i = \mathbf{0}$ , the three intermediate points are analytically derived by iterating three times the rolling primitive  $\mathbf{R}(l, \alpha)$ , through the following parameters:  $l_1 = \rho\pi - \rho\phi, \alpha_1 = \theta; l_2 = \rho\pi, \alpha_2 = \frac{\theta - \psi}{2}; l_3 = 2\pi n\rho, \alpha_3 = \frac{\pi}{2} - \delta$ , in which  $\delta = \arctan 2(y - y_2, x - x_2) - \arccos(d_2/(4\pi n\rho))$ , with  $d_2 = \sqrt{(x - x_2)^2 + (y - y_2)^2}$ . The assumption  $n \geq \frac{d_2}{4\pi n\rho}$  is employed to correctly define the  $\arccos(\cdot)$  function. Finally, a trajectory has to be designed upon the resulting Cartesian path.

#### IV. PH MODELING OF THE ROLLING SYSTEM

In this section, the dynamics of the system is derived using the pH formalism (see Appendix I). The main frames and vectors employed to model the system are depicted in Fig. 4.

In order to include the pure rolling assumption into the model, two constraints are imposed. First, the sphere is not assumed to slip on the plate, meaning that the velocity of the sphere along the  $\hat{x}_p$  and  $\hat{y}_p$  axes is coupled to the rotational velocity of the sphere around the  $\hat{y}_p$  and  $\hat{x}_p$  axes, respectively. Moreover, the sphere is assumed not to spin around the  $\hat{z}_p$  axis of  $\Sigma_p$ . Denoting with  $\boldsymbol{\omega}_b^p = [\omega_x \ \omega_y \ \omega_z]^T$  the

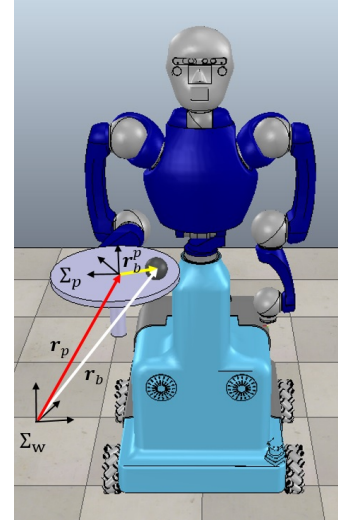


Fig. 4. Schematic view of the position of the sphere both in  $\Sigma_w$  ( $\mathbf{r}_b$  vector in white) and in  $\Sigma_p$  ( $\mathbf{r}_b^p$  vector in yellow), and of the position of the plate in  $\Sigma_w$  ( $\mathbf{r}_p$  vector in red).

angular velocity of the sphere in  $\Sigma_p$ , these constraints are imposed as follows

$$\omega_x = -\rho\dot{y}, \quad \omega_y = \rho\dot{x}, \quad \omega_z = 0. \quad (1)$$

The dynamic model has to take into account also the plate dynamics. In general, the plate has 6 degrees of freedom (dofs), and thus it might be actuated in multiple ways. Nevertheless, not all of them are doable from a control viewpoint. In the following, it is proved that the dynamics of the nonprehensile ball and plate system, with the plate actuated by two horizontal linear forces, is not controllable for the case in which the plate is actuated by two torques around the same horizontal axes. Other combinations might be in principle investigated.

#### A. Force-Controlled Plate

In this first formulation, the plate is actuated by two horizontal linear forces. The frame  $\Sigma_p$  can then only translate with respect to  $\Sigma_w$ , while the relative orientation is kept fixed  $\mathbf{R}_p = \mathbf{I}_3$ , with  $\mathbf{I}_n \in \mathbb{R}^{n \times n}$  the identity matrix. Without loss of generality, the position of the plate in  $\Sigma_w$  is denoted with  $\mathbf{r}_p = [x_p \ y_p \ 0]^T$ , while the configuration vector is given by  $\mathbf{q}_t = [x \ y \ x_p \ y_p]^T$ . Looking at Fig. 4, the position of the sphere in  $\Sigma_w$  can be computed as

$$\mathbf{r}_b = \mathbf{r}_p + \mathbf{R}_p \mathbf{r}_b^p = \mathbf{r}_p + \mathbf{r}_b^p, \quad (2)$$

while the angular velocity of the sphere in  $\Sigma_w$  is  $\boldsymbol{\omega}_b = \boldsymbol{\omega}_b^p$ . The kinetic co-energy of the system is equal to

$$\mathcal{T}_t^* = \frac{1}{2}(m\dot{\mathbf{r}}_b^T \dot{\mathbf{r}}_b + j\boldsymbol{\omega}_b^T \boldsymbol{\omega}_b + m_p \dot{\mathbf{r}}_p^T \dot{\mathbf{r}}_p), \quad (3)$$

where  $m, m_p \in \mathbb{R}$  are the mass of the sphere and the mass of the plate, respectively, while  $j = 2m\rho^2/5$  is the inertia of the sphere. The corresponding mass matrix is obtained

including the pure rolling assumption (1), and folding (2) into the kinetic co-energy (3), yielding

$$\mathbf{M}_t = \begin{bmatrix} \frac{b_0}{\rho} & 0 & m & 0 \\ 0 & \frac{b_0}{\rho} & 0 & m \\ m & 0 & m + m_p & 0 \\ 0 & m & 0 & m + m_p \end{bmatrix}, \quad (4)$$

with  $b_0 = \frac{m\rho^2 + j}{\rho}$ . The input mapping matrix,  $\mathbf{G}_t = [\mathbf{g}_{t1} \ \mathbf{g}_{t2}]$ , with  $\mathbf{g}_{t1} = [0 \ 0 \ 1 \ 0]^T$ ,  $\mathbf{g}_{t2} = [0 \ 0 \ 0 \ 1]^T$ , comes out from the assumption that the plate is actuated through force inputs along the  $\hat{x}$  and  $\hat{y}$  axes of  $\Sigma_w$ . Notice that, since the potential energy is zero in this formulation, by defining the momenta vector as  $\mathbf{p}_t = \mathbf{M}_t \dot{\mathbf{q}}_t$ , this pH system can be modeled as reported in Appendix I. However, as demonstrated in Appendix II, the ball and plate dynamics with horizontal force inputs is not controllable. This is a crucial aspect of dealing with in real experiments especially when performed by robots with limited workspace.

### B. Torque-Controlled Plate

In this formulation, the plate can rotate around the  $\hat{x}$  and  $\hat{y}$  axes of  $\Sigma_w$ , therefore its orientation is included in the system configuration. The position of the plate is now fixed,  $\mathbf{r}_p = \mathbf{0}_3$ , with  $\mathbf{0}_n \in \mathbb{R}^n$  the zero vector. The orientation of the plate in  $\Sigma_w$  is described by the rotation matrix  $\mathbf{R}_p(\phi_p)$ , where  $\phi_p = (\theta_p, \phi_p, \psi_p)$  is the set of ZYX Euler angles. The relation between the time derivative of  $\phi_p$  and its angular velocity in  $\Sigma_w$  is given by

$$\boldsymbol{\omega}_p = \mathbf{R}_p \mathbf{T}_p(\phi_p) \dot{\phi}_p, \quad (5)$$

where  $\mathbf{T}_p(\phi_p) \in \mathbb{R}^{3 \times 3}$  is defined as in [27]. For this formulation, the configuration vector is given by  $\mathbf{q}_r = [x \ y \ \theta_p \ \phi_p]^T$ . The  $\psi_p$  angle around the plate normal direction is fixed. This last constraint on the plate's spin is modeled through the Gimbal equation [27]

$$\dot{\phi}_p \sin \theta_p - \dot{\psi}_p \cos \theta_p \cos \phi_p = 0. \quad (6)$$

Now, the position of the sphere in  $\Sigma_w$  is given by  $\mathbf{r}_b = \mathbf{R}_p \mathbf{r}_b^p$ , while its linear velocity is given by

$$\dot{\mathbf{r}}_b = -S(\mathbf{r}_b) \boldsymbol{\omega}_p + \mathbf{R}_p \dot{\mathbf{r}}_b^p, \quad (7)$$

and its angular velocity is given by

$$\boldsymbol{\omega}_b = \boldsymbol{\omega}_p + \mathbf{R}_p \boldsymbol{\omega}_b^p. \quad (8)$$

The kinetic co-energy of the system is modified as

$$\mathcal{T}_r^* = \frac{1}{2} (m \dot{\mathbf{r}}_b^T \dot{\mathbf{r}}_b + j \boldsymbol{\omega}_b^T \boldsymbol{\omega}_b + \boldsymbol{\omega}_p^T \mathbf{R}_p \mathbf{J}_p \mathbf{R}_p^T \boldsymbol{\omega}_p), \quad (9)$$

where  $\mathbf{J}_p = \text{diag}(j_p^x, j_p^y, j_p^z)$  is the inertia matrix of the plate. In this case, the potential energy of the system is equal to  $\mathcal{V}_r(\mathbf{q}_r) = mg(e_3^T \mathbf{r}_b - \rho)$ , where  $e_i \in \mathbb{R}^3$  has 1 at the  $i$ -th component and 0 otherwise, and  $g \in \mathbb{R}$  is the gravity acceleration. Finally, the input mapping matrix  $\mathbf{G}_r(\mathbf{q}_r) = [\mathbf{g}_{r1} \ \mathbf{g}_{r2}]$ , with  $\mathbf{g}_{r1} = [0 \ 0 \ 1 \ 0]^T$ ,  $\mathbf{g}_{r2} = [0 \ 0 \ 0 \ \cos \theta_p]^T$ , comes out from the assumption that the plate is actuated with torque inputs around the  $\hat{x}$  and  $\hat{y}$

axes of  $\Sigma_w$ . Including the pure rolling assumption (1) and the Gimbal equation (6), folding (5), (7), (8) into the kinetic co-energy (9) yields the following mass matrix

$$\mathbf{M}_r(\mathbf{q}_r) = \begin{bmatrix} \frac{b_0}{\rho} & 0 & 0 & \frac{b_0}{c_{\theta_p}} \\ 0 & \frac{b_0}{\rho} & -b_0 & b_0 m_2 \\ 0 & -b_0 & m_3 & -\frac{mxy}{c_{\theta_p}} - m_3 m_2 \\ \frac{b_0}{c_{\theta_p}} & b_0 m_2 & -\frac{mxy}{c_{\theta_p}} - m_3 m_2 & \frac{m_0}{2c_{\theta_p}^2} \end{bmatrix}, \quad (10)$$

where  $m_0 = 2j_p^x s_{\theta_p}^2 t_{\phi_p}^2 + 2j_p^y + jm_1 + m(m_1 \rho^2 + 2(x + s_{\theta_p} t_{\phi_p} y)^2)$ ,  $m_1 = 2\frac{s_{\theta_p}^2}{c_{\phi_p}^2} + c_2 \theta_p + 1$ ,  $m_2 = t_{\theta_p} t_{\phi_p}$ ,  $m_3 = j_p^x + b_0 \rho + my^2$ ,  $t_{(\cdot)} = \tan(\cdot)$ ,  $c_{(\cdot)} = \cos(\cdot)$ , and  $s_{(\cdot)} = \sin(\cdot)$ . Let  $\mathbf{p}_r = \mathbf{M}_r(\mathbf{q}_r) \dot{\mathbf{q}}_r$  be the definition of the momenta vector, the corresponding pH dynamics is

$$\begin{aligned} \dot{\mathbf{q}}_r &= \nabla_{\mathbf{p}_r} \mathcal{H}(\mathbf{q}_r, \mathbf{p}_r), \\ \dot{\mathbf{p}}_r &= -\nabla_{\mathbf{q}_r} \mathcal{H}(\mathbf{q}_r, \mathbf{p}_r) + \mathbf{G}_r(\mathbf{q}_r) \mathbf{u}_r, \end{aligned} \quad (11)$$

with output vector  $\mathbf{y}_r = \mathbf{G}_r(\mathbf{q}_r)^T \nabla_{\mathbf{q}_r} \mathcal{H}(\mathbf{q}_r, \mathbf{p}_r)$ , and Hamiltonian function  $\mathcal{H}_r(\mathbf{q}_r, \mathbf{p}_r) = \frac{1}{2} \mathbf{p}_r^T \mathbf{M}_r^{-1}(\mathbf{q}_r) \mathbf{p}_r + \mathcal{V}_r(\mathbf{q}_r)$ . The controllability analysis is presented in Appendix II, and it guarantees that both the plate orientation and the sphere position are small-time locally controllable (STLC). This motivates the choice to have the control authority at the torque level for the plate.

### V. CARTESIAN TRAJECTORY TRACKING

In the previous stage, a complete trajectory is available to link the initial and the final position and orientation configurations of the sphere. A Cartesian trajectory tracking technique based on the passivity control theory is now proposed for the ball and plate system to track the path  $\bar{\mathbf{q}}_d(t), \dot{\bar{\mathbf{q}}}_d(t), \ddot{\bar{\mathbf{q}}}_d(t) \in \mathbb{R}^2$  resulting from the geometric trajectory planner presented in Section III.

For control design purposes, it is supposed that the rolling dynamics is slower than the typical frequencies used for the motion control of robot manipulators. Since the torque-controlled plate is firmly attached to the robot manipulator, it is suitable to consider a time-scale separation between the torque control of the plate and the restricted dynamics of the ball on the plate. Therefore, the robot manipulator is equipped with a high-gain motion controller and, neglecting the effects on the tracking errors deriving from the manipulator dynamics, it can be considered as an ideal positioning device [27]. Hence, only the following dynamic model, restricted to the ball rolling on the plate, is considered  $\dot{\bar{\mathbf{q}}} = \nabla_{\bar{\mathbf{p}}} \bar{\mathcal{H}}(\bar{\mathbf{p}})$ ,  $\dot{\bar{\mathbf{p}}} = \bar{\mathbf{u}}$ , with  $\bar{\mathbf{p}} = \mathbf{M} \dot{\bar{\mathbf{q}}}$ , Hamiltonian function  $\bar{\mathcal{H}}(\bar{\mathbf{p}}) = \frac{1}{2} \bar{\mathbf{p}}^T \mathbf{M}^{-1} \bar{\mathbf{p}}$  and mass matrix  $\mathbf{M} = (m + \frac{j}{\rho}) \mathbf{I}_2$ . The (virtual) inputs  $\bar{\mathbf{u}}$  are now some fictitious linear forces acting directly on the sphere. A mapping has then to be found to link  $\bar{\mathbf{u}}$  to the real rotations of the plate.

The IPBC controller for the Cartesian tracking of the sphere on the plate is derived in the next subsection, while the allocation mapping is found in Section V-B.

### A. Integral Passivity-Based Control

Exploiting the tracking control approach in [28] for pH systems, the following control law is proposed

$$\bar{\mathbf{u}} = \mathbf{M}\ddot{\bar{\mathbf{q}}}_d(t) - k_p\tilde{\mathbf{q}} - k_d\mathbf{M}^{-1}\dot{\tilde{\mathbf{p}}} + \mathbf{u}_i, \quad (12)$$

where  $\tilde{\mathbf{q}} = \bar{\mathbf{q}} - \bar{\mathbf{q}}_d(t)$ ,  $\tilde{\mathbf{p}} = \bar{\mathbf{p}} - \bar{\mathbf{p}}_d(t)$  with  $\bar{\mathbf{p}}_d(t) = \mathbf{M}\dot{\bar{\mathbf{q}}}_d(t)$ ,  $k_p, k_d > 0$  are tuning parameters, and  $\mathbf{u}_i$  is an additional control input to be used for integral action. The resulting closed-loop pH dynamics is given by

$$\begin{aligned} \dot{\tilde{\mathbf{q}}} &= \nabla_{\tilde{\mathbf{p}}}\tilde{\mathcal{H}}(\tilde{\mathbf{q}}, \tilde{\mathbf{p}}), \\ \dot{\tilde{\mathbf{p}}} &= -\nabla_{\tilde{\mathbf{q}}}\tilde{\mathcal{H}}(\tilde{\mathbf{q}}, \tilde{\mathbf{p}}) - k_d\nabla_{\tilde{\mathbf{p}}}\tilde{\mathcal{H}}(\tilde{\mathbf{q}}, \tilde{\mathbf{p}}) + \mathbf{u}_i, \end{aligned} \quad (13)$$

with output vector  $\mathbf{y} = \nabla_{\tilde{\mathbf{p}}}\tilde{\mathcal{H}}$ , and Hamiltonian function  $\tilde{\mathcal{H}}(\tilde{\mathbf{q}}, \tilde{\mathbf{p}}) = \frac{1}{2}\tilde{\mathbf{p}}^T\mathbf{M}^{-1}\tilde{\mathbf{p}} + \frac{k_p}{2}\tilde{\mathbf{q}}^T\tilde{\mathbf{q}}$ . This system is asymptotically stable to the equilibrium  $\tilde{\mathbf{q}} = \mathbf{0}$ ,  $\tilde{\mathbf{p}} = \mathbf{0}$ . Using the control law (12), the system configuration asymptotically converges to the pre-planned Cartesian path,  $\bar{\mathbf{q}} = \bar{\mathbf{q}}_d(t)$ ,  $\bar{\mathbf{p}} = \bar{\mathbf{p}}_d(t)$ . The term  $\mathbf{u}_i$  in (12) is used to add integral action exploiting the scheme proposed in [11]. Here a damping term  $k_{di}$  has been added to improve the transient performance. The integral control action has the following form

$$\begin{aligned} \mathbf{u}_i &= -k_d k_i(\tilde{\mathbf{p}} - \boldsymbol{\zeta}) - k_{di}\mathbf{M}^{-1}\dot{\tilde{\mathbf{p}}}, \\ \dot{\boldsymbol{\zeta}} &= -k_p\tilde{\mathbf{q}} - k_{di}\mathbf{M}^{-1}\tilde{\mathbf{p}}, \end{aligned} \quad (14)$$

where  $\boldsymbol{\zeta} \in \mathbb{R}^2$  is an additional integral state and  $k_i, k_{di} > 0$  are integral gains. Including the integral control (14) and neglecting the dependencies, the closed-loop dynamics become

$$\begin{aligned} \dot{\tilde{\mathbf{q}}} &= \nabla_{\tilde{\mathbf{p}}}\tilde{\mathcal{H}}_{cl} + \nabla_{\boldsymbol{\zeta}}\tilde{\mathcal{H}}_{cl}, \\ \dot{\tilde{\mathbf{p}}} &= -\nabla_{\tilde{\mathbf{q}}}\tilde{\mathcal{H}}_{cl} - (k_d + k_{id})\nabla_{\tilde{\mathbf{p}}}\tilde{\mathcal{H}}_{cl} - k_{id}\nabla_{\boldsymbol{\zeta}}\tilde{\mathcal{H}}_{cl}, \\ \dot{\boldsymbol{\zeta}} &= -\nabla_{\tilde{\mathbf{q}}}\tilde{\mathcal{H}}_{cl} - k_{id}\nabla_{\tilde{\mathbf{p}}}\tilde{\mathcal{H}}_{cl} - k_{id}\nabla_{\boldsymbol{\zeta}}\tilde{\mathcal{H}}_{cl}, \end{aligned} \quad (15)$$

with the closed-loop energy function  $\tilde{\mathcal{H}}_{cl} = \frac{1}{2}\tilde{\mathbf{p}}^T\mathbf{M}^{-1}\tilde{\mathbf{p}} + \frac{k_p}{2}\tilde{\mathbf{q}}^T\tilde{\mathbf{q}} + \frac{k_i}{2}(\tilde{\mathbf{p}} - \boldsymbol{\zeta})^T(\tilde{\mathbf{p}} - \boldsymbol{\zeta})$ .

Stability is established by taking  $\tilde{\mathcal{H}}_{cl}$  as a Lyapunov candidate for the closed loop system. Along the trajectories of the system, the time derivative of  $\tilde{\mathcal{H}}_{cl}$  satisfies  $\dot{\tilde{\mathcal{H}}}_{cl} = -k_d(\nabla_{\tilde{\mathbf{p}}}^T\tilde{\mathcal{H}}_{cl})^T(\nabla_{\tilde{\mathbf{p}}}^T\tilde{\mathcal{H}}_{cl}) - k_{id}(\nabla_{\tilde{\mathbf{p}}}^T\tilde{\mathcal{H}}_{cl} - \nabla_{\boldsymbol{\zeta}}^T\tilde{\mathcal{H}}_{cl})^T(\nabla_{\tilde{\mathbf{p}}}^T\tilde{\mathcal{H}}_{cl} - \nabla_{\boldsymbol{\zeta}}^T\tilde{\mathcal{H}}_{cl})$ . Asymptotic stability follows by invoking LaSalle's invariance principle.

Such IPBC technique offers some benefits compared with a PID-based controller, as explained in Subsection VI-A.

### B. Control Allocation

In order to map the fictitious forces acting on the sphere into the plate motion, a control allocation is employed. The force due to gravity, expressed in  $\Sigma_w$ , can be described by the vector  $\mathbf{f}_g = [0 \ 0 \ -mg]^T$ . Then, the forces acting on the sphere,  $\bar{\mathbf{u}}$ , are mapped into the forces due to gravity, expressed in  $\Sigma_p$ , through  $\bar{\mathbf{u}} = [u_x \ u_y \ u_z]^T = \mathbf{R}_p^T\mathbf{f}_g$ . Inverting this last equation provides the plate orientation corresponding to the desired forces acting on the sphere:  $\phi_p = \arcsin(u_x/mg)$  and  $\theta_p = \arcsin(-u_y/mg \cos \phi_p)$ . The  $u_x$  and  $u_y$  terms are given by the IPBC law (12), while  $u_z$  is arbitrary, as it will be canceled out by the reaction forces of the plate.

## VI. EXPERIMENTS

Instead of building a proper simpler set-up on purpose, the experiments are performed on the available 21-dof humanoid-like robot displayed in Fig. 2 [29]. This robot is equipped with a 2-dof torso, two 7-dof arms, a 2-dof neck, a head, and a mobile base, and it is properly designed to test control approaches for nonprehensile manipulation tasks. For this application, the right arm is equipped with a plate firmly attached at its end-effector. The size of the square plate is 0.4 m  $\times$  0.4 m  $\times$  0.005 m. The dynamic parameters of the physical rolling sphere-plate system are:  $m = 0.216$  kg,  $\rho = 0.035$  m and  $m_p = 1.3$  kg. The processing unit of the robot is composed of two computers with a Linux-based operating system, that communicate through a socket. One of the units is provided with a distribution of the QnX system and is dedicated to the low-level control running at 5 ms. In the other unit, the 14.04 version of the Xubuntu system is installed to run the high-level control.

The head is equipped with a 50 Hz stereo-vision system, which tracks the rolling sphere position on the plate and provides the feedback for the control law presented in Section V. In detail, the vision system consists in estimating the 3D location of the center of the ball in one of the stereo camera frames, by triangulating the detected and tracked 2D positions of the ball in both grayscale images. The 2D detection and tracking procedure of the ball relies on Hough-based circle detections on both images. The detected circles are then used to initialize, or reinitialize, a frame-by-frame circle-tracking technique which consists in locally fitting the circles on edges extracted in the images. This method employs the *moving edge* algorithm [30] to match projected boundaries of the tracked 3D ball with extracted edges from both images. To cope with outliers, an iteratively re-weighted least squares optimization with respect to 2D circle parameters (center and radius), with Tukey M-estimators, is used. The implementation is based on both OpenCV<sup>2</sup> and ViSP [31] libraries.

A Kalman filter is exploited to reduce the sensitivity to noise in the velocity computation, obtained from the position measurements. Finally, a trapezoidal acceleration trajectory [27], with a piece-wise constant jerk, is implemented along the path coming from the planner. By choice, the ball stops at each intermediate point. Nevertheless, if three consecutive intermediate points belong to the same straight line, the ball stops only at the first and the last one.

### A. Comparative Regulation Test

This experiment is performed to compare the proposed IPBC approach with a classical PID method. The latter is designed instead from a traditional Lagrangian model of a ball rolling on a plate. Such Lagrangian model can be retrieved by applying the Legendre transformation to the pH model. The controlling purpose is to bring the sphere at the plate's center  $\bar{\mathbf{q}}_d = [0 \ 0]^T$  m starting from a different initial position. Naturally, the geometric trajectory planning

<sup>2</sup><https://opencv.org/>

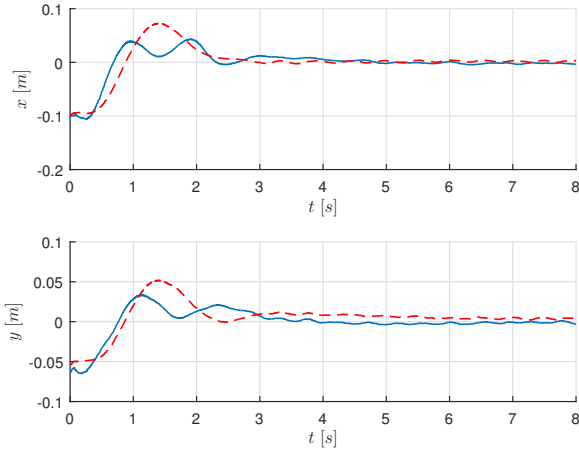


Fig. 5. Sphere position in  $\Sigma_p$  resulting from the PID control (dashed red line) and the IPBC (solid blue line).

phase is not included in this test, since the sphere is not reoriented. Initially, the sphere is manually placed on the plate, and its initial position  $\bar{q}(0)$  in  $\Sigma_p$  corresponds to the first position measurement. Such  $\bar{q}(0)$  is chosen as much close as possible in both the tests employing the PID and IPBC controllers.

Regarding the test with the PID controller, the initial position is  $\bar{q}(0) = [-0.09762 \quad -0.05354]^T$  m. The chosen values for the proportional, derivative and integral gains are  $k'_p = 5.4$ ,  $k'_d = 1.8$  and  $k'_i = 1.7$ , respectively. Whereas, for the evaluation of the IPBC technique, the initial condition is  $\bar{q}(0) = [-0.09906 \quad -0.06283]^T$  m, while the IPBC gains are tuned as  $k_p = 1.1$ ,  $k_d = 0.6$ ,  $k_i = 1.2$ , and  $k_{di} = 0.2$ . The gains have been experimentally tuned to the best of the authors' ability to achieve similar settling times in both tests.

The obtained comparison between the proposed IPBC technique and the classical PID controller is depicted in Fig. VI-A. A smaller overshoot is visible in the IPBC controller for the PID technique. The steady-state position error with the IPBC approach is about half than the one obtained with the PID controller. Additionally, notice that a PID control law, applied to the ball and plate system, provides asymptotic stability only for a limited set of the positive  $k'_p$ ,  $k'_d$  and  $k'_i$  gains, namely  $k'_p k'_d > k'_i$ , according to Hurwitz's criterion. Instead, the proposed IPBC technique is theoretically stable for all possible positive gains  $k_p, k_d, k_i, k_{di} > 0$ .

### B. Pose Reconfiguration Test

The geometric trajectory planning phase is now duly addressed within the two different reconfiguration tests described in the following.

1) *Test 1*: In this test, the initial position of the sphere is  $\bar{q}(0) = [0.08015 \quad -0.04703]^T$  m and, without loss of generality, the initial orientation is assumed equal to the identity. The initial and final velocities of the sphere are assumed to be zero, while the desired position is  $\bar{q}_d =$

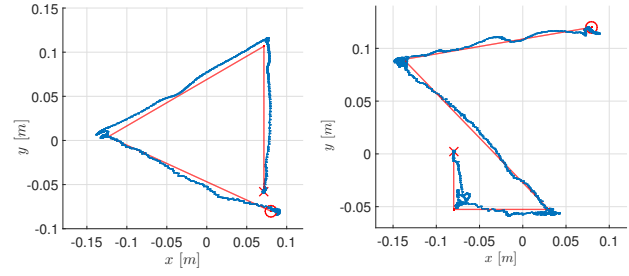


Fig. 6. Position and orientation reconfiguration - test 1 (left) and test 2 (right). Pre-planned sphere Cartesian path,  $\bar{q}_d$  (red line), and actual Cartesian path,  $\bar{q}$  (blue line). The starting point is marked by a cross, while the final goal is denoted as a circle.

$[0.08 \quad -0.08]^T$  m and the desired orientation is given by the rotation matrix  $\mathbf{R}_d = [e_1 \quad e_3 \quad -e_2]$ . Following the proposed approach, the geometric trajectory planner provides the three intermediate points of the pre-planned path:  $\bar{q}_1 = [0.0801 \quad 0.0079]^T$  m,  $\bar{q}_2 = [0.0801 \quad 0.1179]^T$  m, and  $\bar{q}_3 = [-0.1163 \quad 0.0191]^T$  m. As mentioned before, since  $\bar{q}_i$ , with  $i = 0, 1, 2$ , belong to a straight line, the ball does not stop at  $\bar{q}_1$ . The left picture of Fig. 6 depicts the planned Cartesian path and the actual position trajectory of the sphere, in  $\Sigma_p$ , resulting from the application of the IPBC. As confirmed by the norm of the linear position and momenta errors, shown in Fig. 8(a), the IPBC provides good tracking performance: the position tracking error norm is under 2.5 cm. This error is mainly due to unmodeled dynamics, such as static friction at the beginning, small deformation of the surfaces in contact, or error due to the measurement system. The IPBC gains are tuned for this tracking test as  $k_p = 1.9$ ,  $k_d = 0.6$ ,  $k_i = 0.6$ , and  $k_{di} = 0.1$ . Fig. 8(a) also shows the evolution of the  $\phi_p$  and  $\theta_p$  plate angles resulting from the control allocation phase. Finally, the orientation error is evaluated at the final time, when the sphere must be effectively reoriented. In this test, the orientation error<sup>3</sup> is  $d_r = 0.34$  rad, which is a fair result, as it can be appreciated in the video attachment<sup>4</sup> and Fig. 7.

2) *Test 2*: A second reconfiguration test is performed to accomplish the task with a different desired pose for the sphere. In this case, the initial pose of the sphere is  $\bar{q}(0) = [-0.07989 \quad 0.002352]^T$  m, and  $\mathbf{R}(0) = \mathbf{I}_3$ . Whereas, the desired position and orientation of the sphere are  $\bar{q}_d = [0.08 \quad 0.12]^T$  m, and  $\mathbf{R}_d = [-e_1 \quad -e_3 \quad -e_2]$ , respectively. As shown in the right picture of Fig. 6, the three intermediate points, obtained from the geometric path planner, are:  $\bar{q}_1 = [-0.0799 \quad -0.0526]^T$  m,  $\bar{q}_2 = [-0.1898 \quad -0.0526]^T$  m, and  $\bar{q}_3 = [0.0263 \quad -0.0932]^T$  m. The right picture of Fig. 6 depicts the pre-planned Cartesian path and the actual position trajectory of the sphere in  $\Sigma_p$ . The norm of the linear

<sup>3</sup>The orientation error is evaluated through the geodesic metric on  $\text{SO}(3)$ :  $d_r = 1/\sqrt{2} \|\log(\mathbf{R}^T \mathbf{R}_d)\|_F$  rad, where  $\mathbf{R}_d, \mathbf{R} \in \text{SO}(3)$  are, respectively, the desired and the current rotation matrices, and  $\|\cdot\|_F$  is the Frobenius norm [32].

<sup>4</sup><https://youtu.be/3m9552fV2QU>

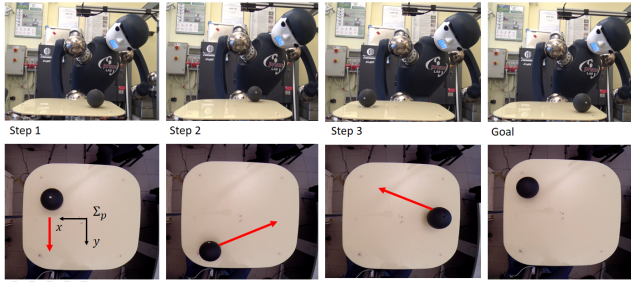
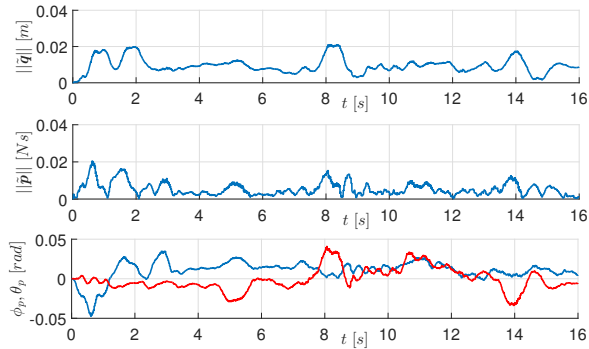
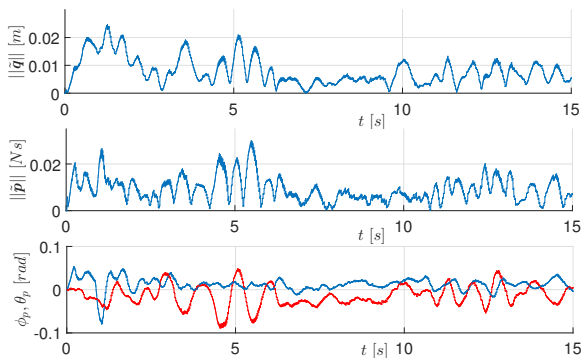


Fig. 7. Pictures of the steps to reconfigure the sphere pose for the test 1. The top (bottom) pictures display the front (top) view. The red vectors indicate, step by step, the planned direction of the path to be covered by the sphere. The white marker on the sphere helps the reader and the operator to understand its reorientation. The marker is indeed not used by the vision system, but it is instead useful to roughly appreciate the changes in the orientation of the sphere.



(a) Test 1.



(b) Test 2.

Fig. 8. Position and orientation reconfiguration. IPBC tracking error:  $\|\hat{q}\|$  (top picture) and  $\|\hat{p}\|$  (middle picture). Angular position of the plate resulting from the control allocation (bottom picture):  $\phi_p$  angle (blue line) and  $\theta_p$  angle (red line).

position and momenta errors, shown in Fig. 8(b), confirms the validity of the control technique again. The same gains from the previous test are used. The position tracking error is still always under 2.5 cm. The Fig. 8(b) also shows the evolution of the  $\phi_p$  and  $\theta_p$  plate angles. The orientation error, evaluated only at the final time, is now  $d_r = 0.1$  rad, confirming that the sphere has been correctly reoriented, as it can also be appreciated in the video attachment.

## VII. CONCLUSION AND FUTURE WORK

An experimental approach for the problem of the nonprehensile rolling manipulation of a sphere on a plate is proposed here. The experimental results display the robustness and the performance of the proposed approach.

The inclusion of an offline optimization would provide the path minimizing some specific cost term, such as the length of the path covered by the sphere, or the control effort. An optimal planner can be conceived solving a two-boundary value problem, as proposed in [33]. Moreover, by exploiting the controllability analysis within Appendix II and the dynamic model (11) in Subsection IV-B, a proper controller can be found for this system without explicitly using the time-scale separation property, despite this is most likely correct among the available robotic set-ups. Moreover, the pure rolling assumption is supposed so far: building a controller by taking into account the friction between the sphere and the plate to prevent slippage is an attractive improvement. Finally, the offline planned path might be refined in runtime.

## APPENDIX I: PORT-HAMILTONIAN MODELING

Mechanical systems can be modeled through the pH formalism including the information about the energy transfer explicitly. The Hamilton canonical equations of motion are given by

$$\begin{aligned} \dot{q} &= \nabla_p \mathcal{H}(q, p) \\ \dot{p} &= -\nabla_q \mathcal{H}(q, p) + G(q)u \end{aligned} \quad (16)$$

with output vector  $y = G(q)^T \nabla_q \mathcal{H}(q, p)$ , and Hamiltonian function  $\mathcal{H}(q, p) = \frac{1}{2} p^T M^{-1}(q) p + \mathcal{V}(q)$ , where  $p \in \mathbb{R}^n$  is the generic momenta vector,  $q \in \mathbb{R}^n$  is the generic configuration vector,  $M(q)$  is the symmetric and positive definite mass matrix,  $\mathcal{V}(q)$  is the potential energy function, and  $G(q)$  is the input mapping matrix [34]. The resulting closed-loop pH system is passive considering  $u$  as input,  $y$  as output, and the Hamiltonian  $\mathcal{H}$  as storage function.

## APPENDIX II: CONTROLLABILITY ANALYSIS

The sphere-plate dynamics presented in Subsection IV-A is a linear time-invariant (LTI) system that can be represented in the state-space form as

$$\dot{x}_t = A_t x_t + B_t u_t, \quad (17)$$

where  $x_t = [q_t^T \ p_t^T]^T$  and  $u_t \in \mathbb{R}^2$  is the input force vector.  $A_t \in \mathbb{R}^{8 \times 8}$  and  $B_t \in \mathbb{R}^{8 \times 2}$  depend on  $M_t$  and  $G_t$ . Employing the Kalman rank condition for LTI systems, the sphere-plate dynamics with force inputs (17) results not

controllable since  $\text{rank}(\mathbf{K}_t) = 4 < 8$ , where  $\mathbf{K}_t \in \mathbb{R}^{8 \times 16}$  is the Kalman controllability matrix of (17).

On the other hand, the dynamics (11) presented in Subsection IV-B can be represented in the nonlinear state-space form

$$\dot{\mathbf{x}}_r = \mathbf{h}(\mathbf{x}_r, \mathbf{u}_r), \quad (18)$$

where  $\mathbf{x}_r = [\mathbf{q}_r^T \ \mathbf{p}_r^T]^T$  and  $\mathbf{u}_r \in \mathbb{R}^2$  is the input torque vector.  $\mathbf{h}(\cdot) \in \mathbb{R}^8$  is a vector function related to the matrices  $\mathbf{M}_r$  and  $\mathbf{G}_r$ . The nonlinear dynamics (18) is a control-affine system satisfying the assumption of vanishing drift at initial state. Subsequently, employing the STLC criterion in [35], the dynamics (11) is STLC from the initial state if its linearization

$$\dot{\mathbf{x}}_r = \mathbf{A}_r \mathbf{x}_r + \mathbf{B}_r \mathbf{u}_r, \quad (19)$$

with  $\mathbf{A}_r \in \mathbb{R}^{8 \times 8}$  and  $\mathbf{B}_r \in \mathbb{R}^{8 \times 2}$ , is STLC from zero. Let  $\mathbf{K}_r \in \mathbb{R}^{8 \times 16}$  be the corresponding Kalman controllability matrix, the rank condition for LTI systems is now satisfied, since  $\text{rank}(\mathbf{K}_r) = 8$ . Consequently, the sphere-plate dynamics with torque inputs is STLC.

Full expressions of the presented terms and detailed computations are omitted for brevity.

#### REFERENCES

- [1] M. Mason and K. Lynch, "Dynamic manipulation," in *1993 IEEE/RSJ International Conference on Intelligent Robots and Systems*, Yokohama, J, 1993, pp. 152–159.
- [2] F. Ruggiero, V. Lippiello, and B. Siciliano, "Nonprehensile dynamic manipulation: A survey," *IEEE Robotics and Automation Letters*, vol. 3, no. 3, pp. 1711–1718, 2018.
- [3] K. M. Lynch, N. Shiroma, H. Arai, and K. Tanie, "The roles of shape and motion in dynamic manipulation: The butterfly example," in *IEEE International Conference on Robotics and Automation*, vol. 3, Leuven, BE, 1998, pp. 1958–1963.
- [4] P. Choudhury and K. M. Lynch, "Rolling manipulation with a single control," *The International Journal of Robotics Research*, vol. 21, no. 5-6, pp. 475–487, 2002.
- [5] D. Serra, A. Satici, F. Ruggiero, V. Lippiello, and B. Siciliano, "An optimal trajectory planner for a robotic batting task: the table tennis example," in *International Conference on Informatics in Control, Automation and Robotics*, Lisbon, P, 2016, pp. 90–101.
- [6] D. Serra, A. C. Satici, F. Ruggiero, V. Lippiello, and B. Siciliano, "Time-optimal paths for a robotic batting task," *Springer Lecture Notes in Electrical Engineering*, p. to appear, 2017.
- [7] D. Serra, F. Ruggiero, V. Lippiello, and B. Siciliano, "A nonlinear least squares approach for nonprehensile dual-hand robotic ball juggling," in *World Congress of the International Federation of Automatic Control*, Toulouse, FR, 2017.
- [8] D. Serra, "Robot control for nonprehensile dynamic manipulation tasks," in *International Conference on Informatics in Control, Automation and Robotics, Doctoral Consortium*, Lisbon, P, 2016.
- [9] K. M. Lynch and M. T. Mason, "Dynamic nonprehensile manipulation: Controllability, planning, and experiments," *The International Journal of Robotics Research*, vol. 18, no. 1, pp. 64–92, 1999.
- [10] A. M. Bloch, M. Reyhanoglu, and N. H. McClamroch, "Control and stabilization of nonholonomic dynamic systems," *IEEE Transactions on Automatic Control*, vol. 37, no. 11, pp. 1746–1757, 1992.
- [11] J. Ferguson, A. Donaire, and R. Middleton, "Integral control of port-hamiltonian systems: Non-passive outputs without coordinate transformation," *IEEE Transaction on Automatic Control*, p. to appear, 2017.
- [12] D. J. Montana, "The kinematics of contact and grasp," *The International Journal of Robotics Research*, vol. 7, no. 3, pp. 17–32, 1988.
- [13] R. M. Murray, Z. Li, and S. S. Sastry, *A mathematical introduction to robotic manipulation*. CRC press, 1994.
- [14] V. Jurdjevic, "The geometry of the plate ball problem," *Archive for Rational Mechanics and Analysis*, vol. 124, no. 4, pp. 305–328, 1993.
- [15] A. Becker and T. Bretl, "Approximate steering of a plate ball system under bounded model perturbation using ensemble control," in *IEEE International Conference on Intelligent Robots and Systems*, Vilamoura, PT, 2012, pp. 5353–5359.
- [16] A. Bicchi and R. Sorrentino, "Dexterous manipulation through rolling," in *IEEE International Conference on Robotics and Automation*, vol. 1, Nagoya, J, 1995, pp. 452–457.
- [17] A. Bicchi, A. Marigo, and D. Prattichizzo, "Dexterity through rolling: Manipulation of unknown objects," in *IEEE International Conference on Robotics and Automation*, vol. 2, Detroit, MI, USA, 1999, pp. 1583–1588.
- [18] A. Marigo and A. Bicchi, "Rolling bodies with regular surface: Controllability theory and applications," *IEEE Transactions on Automatic Control*, vol. 45, no. 9, pp. 1586–1599, 2000.
- [19] K. K. Lee, G. Batz, and D. Wollherr, "Basketball robot: Ball on plate with pure haptic information," in *IEEE International Conference on Robotics and Automation*, Pasadena, CA, USA, 2008, pp. 2410–2415.
- [20] K. Harada and M. Kaneko, "Rolling based manipulation under neighborhood equilibrium," in *IEEE International Conference on Robotics and Automation*, vol. 3, Seoul, K, 2001, pp. 2492–2498.
- [21] K. Harada and M. Kaneko, "Neighborhood equilibrium grasp for multiple objects," in *IEEE International Conference on Robotics and Automation*, vol. 3, San Francisco, CA, USA, 2000, pp. 2159–2164.
- [22] L. Cui and J. S. Dai, "A coordinate-free approach to instantaneous kinematics of two rigid objects with rolling contact and its implications for trajectory planning," in *IEEE International Conference on Robotics and Automation*, Kobe, J, 2009, pp. 612–617.
- [23] H. Date, M. Sampei, M. Ishikawa, and M. Koga, "Simultaneous control of position and orientation for ball plate manipulation problem based on time state control form," *IEEE Transactions on Robotics and Automation*, vol. 20, no. 3, pp. 465–480, 2004.
- [24] G. Oriolo and M. Vendittelli, "A framework for the stabilization of general nonholonomic systems with an application to the plate-ball mechanism," *IEEE Transactions on Robotics*, vol. 21, no. 2, pp. 162–175, 2005.
- [25] T. Das and R. Mukherjee, "Exponential stabilization of the rolling sphere," *Automatica*, vol. 40, no. 11, pp. 1877–1889, 2004.
- [26] D. Casagrande, A. Astolfi, and T. Parisini, "Switching driving Lyapunov function and the stabilization of the ball and plate system," *IEEE Transactions on Automatic Control*, vol. 54, no. 8, pp. 1881–1886, 2009.
- [27] B. Siciliano, L. Sciacivico, L. Villani, and G. Oriolo, *Robotics: Modelling, Planning and Control*. London, UK: Springer, 2009.
- [28] K. Fujimoto, K. Sakurama, and T. Sugie, "Trajectory tracking control of port-controlled Hamiltonian systems via generalized canonical transformations," *Automatica*, vol. 39, no. 12, pp. 2059–2069, 2003.
- [29] F. Ruggiero, A. Petit, D. Serra, A. Satici, J. Cacace, A. Donaire, F. Ficuciello, L. R. Buonocore, G. A. Fontanelli, V. Lippiello, V. Villani, and B. Siciliano, "Nonprehensile manipulation of deformable objects: Achievements and perspectives from the RoDyMan project," *IEEE Robotics & Automation Magazine*, 2018, DOI: 10.1109/MRA.2017.2781306.
- [30] P. Bouthemy, "A maximum likelihood framework for determining moving edges," *IEEE Transactions on pattern analysis and machine intelligence*, vol. 11, no. 5, pp. 499–511, 1989.
- [31] E. Marchand, F. Spindler, and F. Chaumette, "ViSP for visual servoing: A generic software platform with a wide class of robot control skills," *IEEE Robotics and Automation Magazine*, vol. 12, no. 4, pp. 40–52, 2005.
- [32] D. Huynh, "Metrics for 3d rotations: Comparison and analysis," *Journal of Mathematical Imaging and Vision*, vol. 35, pp. 155–164, 2009.
- [33] R. W. Brockett and L. Dai, "Non-holonomic kinematics and the role of elliptic functions in constructive controllability," in *Nonholonomic motion planning*, 1993, pp. 1–21.
- [34] R. Ortega and E. Garcia-Canseco, "Interconnection and damping assignment passivity-based control: A survey," *European Journal of control*, vol. 10, no. 5, pp. 432–450, 2004.
- [35] F. Bullo and A. D. Lewis, "Kinematic controllability and motion planning for the snakeboard," *IEEE Transactions on Robotics and Automation*, vol. 19, no. 3, pp. 494–498, 2003.